

# First-order transition and marginal critical behavior in a novel 2D frustrated Ising model

Christophe Chatelain

Université de Lorraine, CNRS, LPCT, F-54000 Nancy, France

(Dated: October 3, 2024)

The phase diagram of a novel two-dimensional frustrated Ising model with both anti-ferromagnetic and ferromagnetic couplings is studied using Tensor-Network Renormalization-Group techniques. This model can be seen as two anti-ferromagnetic Ising replicas coupled by non-local spin-spin interactions, designed in such a way that the continuum limit matches that of the still debated  $J_1 - J_2$  model and induces a marginal critical behavior. Our model has the advantage of having more symmetries than the  $J_1 - J_2$  model and of allowing a more straightforward implementation of Tensor-Network Renormalization-Group algorithms. We demonstrate the existence of two transition lines, featuring both first and second-order regimes. In the latter, the central charge and the critical exponents are shown to be compatible with the Ashkin-Teller universality class. This picture is consistent with that given by Monte Carlo simulations of the  $J_1 - J_2$  model but not with recent studies with Tensor-Network techniques.

## I. INTRODUCTION

Despite of decades of active research, the phase diagram of the Ising model with ferromagnetic couplings  $J_1$  between nearest-neighboring spins and anti-ferromagnetic ones  $J_2$  between next-nearest ones remains controversial. On the square lattice, the Hamiltonian of the  $J_1 - J_2$  model is

$$-\beta H = J_1 \sum_{i,j} \sigma_{i,j} [\sigma_{i+1,j} + \sigma_{i,j+1}] - J_2 \sum_{i,j} [\sigma_{i,j} \sigma_{i+1,j+1} + \sigma_{i+1,j} \sigma_{i,j+1}] \quad (1)$$

with  $\sigma_{i,j} \in \{-1; +1\}$ . The ferromagnetic Ising model is recovered when  $J_2 = 0$ . The system undergoes therefore a ferromagnetic-paramagnetic second-order phase transition at the self-dual coupling  $J_1 = \frac{1}{2} \ln(1 + \sqrt{2})$  [1, 2]. The critical behavior belongs to the Ising universality class with magnetic and thermal critical exponents  $\beta = 1/8$  and  $\nu = 1$  and a central charge  $c = 1/2$ . When  $J_1 = 0$ , the system decouples into two sublattices, at  $45^\circ$  of the original lattice and with a lattice step  $\sqrt{2}$  (Fig. 1). Each one of these sublattices undergoes a transition from an anti-ferromagnetic phase to the paramagnetic phase at  $J_2 = \frac{1}{2} \ln(1 + \sqrt{2})$ . The associated critical behavior also belongs to the Ising universality class. The central charge of the model is  $c = 2 \times \frac{1}{2} = 1$ .

For non-zero  $J_1$  and  $J_2$ , the ground state is readily obtained by minimizing the energy of a plaquette of 4 spins. When  $g = J_2/J_1 < 1/2$ , the ground states are the two ferromagnetic spin configurations. In contrast, when  $g > 1/2$ , the ground state is ferromagnetic in one direction of the lattice but anti-ferromagnetic in the other one. The four possible spin configurations show stripes, either horizontal or vertical. These ground-states are sometimes referred to as super-antiferromagnetic. Early transfer-matrix and Monte Carlo simulations suggested the existence of a line of continuous phase

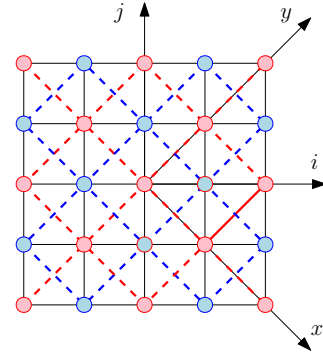


FIG. 1. Ising model with nearest and next-to-nearest couplings. The black edges are the ferromagnetic couplings  $J_1$ . The dashed edges are anti-ferromagnetic with a coupling  $J_2$ . The blue and red colors correspond to the two sublattices that are decoupled when  $J_1 = 0$ .

transition to the paramagnetic phase [3–6]. The critical behavior belongs to the Ising universality class in the regime  $g < 1/2$ , i.e. for the ferromagnetic-paramagnetic transition. However, in the regime  $g > 1/2$ , i.e. for the transition between the super-antiferromagnetic and paramagnetic phases, critical exponents were observed to vary with the ratio  $g$  but the ratio  $\beta/\nu$  remains constant, in agreement with the weak-universality scenario [7]. One decade later, Morán-López *et al.* showed by mean-field calculations the existence of a regime of first-order phase transition when  $1/2 < g \lesssim 1.14$  [8, 9]. Later Monte Carlo simulations confirmed the existence of this regime but only in the range  $1/2 < g \lesssim 0.67$  [10–13].

These studies also agree on the fact that, in the second-order regime  $g \gtrsim 0.67$ , the critical behavior belongs to the Ashkin-Teller universality class. The Ashkin-Teller model consists in two Ising models coupled by their energy densities. This coupling is marginal and leads to non-universal critical exponents [14–16]. As shown on Fig. 1, the  $J_1 - J_2$  Ising model can also be viewed as two

anti-ferromagnetic Ising models that are coupled by a spin-spin interaction, rather than an energy-energy one. However, this interaction does not couple spins at the same site, the perturbation would be irrelevant in that case, but at different sites. Kalz *et al.* argued that this perturbation is marginal, as in the Ashkin-Teller model [10]. Their argument goes as follows. Introduce the spins on the two sublattices as  $\sigma_{x,y}^A$  and  $\sigma_{x,y}^B$  where the lattice coordinates  $(x, y)$  shown on Fig. 1 are integers on the sublattice A and half-integers on B. The total energy associated to the ferromagnetic couplings between the two sublattices reads

$$J_1 \sum_{x,y} \sigma_{x,y}^A [\sigma_{x-1/2,y-1/2}^B + \sigma_{x-1/2,y+1/2}^B + \sigma_{x+1/2,y-1/2}^B + \sigma_{x+1/2,y+1/2}^B]. \quad (2)$$

In the super-antiferromagnetic phase, the two sublattices are anti-ferromagnetically ordered, so it is convenient to introduce the staggered magnetization as

$$S_{x,y}^A = (-1)^{x+y} \sigma_{x,y}^A, \quad S_{x,y}^B = (-1)^{x+y} \sigma_{x,y}^B. \quad (3)$$

In the continuum limit, the energy Eq. 2 tends to

$$J_1 \sum_{x,y} S_{x,y}^A \left[ -S_{x-1/2,y-1/2}^B + S_{x-1/2,y+1/2}^B + S_{x+1/2,y-1/2}^B - S_{x+1/2,y+1/2}^B \right] \simeq -4J_1 \int S^A \partial_x \partial_y S^B dx dy. \quad (4)$$

This term is irrelevant but a perturbative calculation in  $J_1$  shows that two marginal terms are generated at second-order, one of them being an energy-energy coupling  $\varepsilon_{x,y}^A \varepsilon_{x,y}^B$  as in the Ashkin-Teller model.

The situation was rather clear one decade ago. However, recent calculations based on Tensor-Network techniques have called these results into question but have reached opposite conclusions. A first study based on the Higher-Order Tensor Renormalization Group algorithm (HoTRG) [17] observed varying critical exponents but not in the Ashkin-Teller universality class [18]. A second study by HoTRG concluded that the regime of first-order transition is limited to  $1/2 < g \lesssim 0.58$ , i.e. significantly smaller than previously claimed, and that the behavior at the tricritical point does not belong to the 4-state Potts universality class, excluding therefore the Ashkin-Teller universality class along the critical line [19]. A recent Monte Carlo simulation yields the same conclusion on the location of the tricritical point [20]. The  $J_1 - J_2$  model was also studied by simulating the imaginary-time evolution of a Matrix Product State using the iTeBD algorithm [21]. It was observed that the first-order regime extends to  $1/2 < g < +\infty$ , i.e. that the transition becomes continuous only in the limit  $g \rightarrow +\infty$  when  $J_1 = 0$ .

The interest in Tensor-Network Renormalization Group techniques stems from their ability to overcome certain limitations inherent in other computational methods. Transfer matrix calculations are exact but limited to small stripes. Monte Carlo simulations, on the other hand, enable the study of larger systems. However, since there is no cluster algorithm for the  $J_1 - J_2$  model, simulations were performed using the Metropolis algorithm that is known to suffer from a strong critical slowing-down with a dynamical exponent  $z \simeq 2.17$  at the Ising critical point [22]. Monte Carlo simulations at first-order phase transitions are also notoriously difficult because the exponentially small probability of tunneling between the low-temperature phases has to be compensated by an exponentially large number of Monte Carlo iterations (super critical slowing-down). Multicanonical algorithms allow to overcome this difficulty. Tensor-Network techniques open the door to considerably larger lattices. However, these techniques are variational and come with their own set of challenges. Whereas statistical errors can be rigorously estimated for any thermodynamic average computed by Monte Carlo simulation, one can only check the convergence of the estimates obtained with Tensor-Network algorithms by performing calculations with different bond dimensions. Errors on thermodynamic averages cannot be estimated from the truncation error. Moreover, the convergence of Tensor Renormalization Group algorithms depends on the particular decomposition of the partition function into a product of tensors [23].

In this paper, we consider a different  $J_1 - J_2$  model that is more suited to simulations by Tensor Renormalization Group algorithms. The Hamiltonian Eq. 1 requires to either manipulate rank 8 tensors or to consider rank 4 tensors but with non-independent legs. In Ref. [19], a rank 4 tensor is associated to each plaquette of the square lattice. The legs of the tensor do not correspond to the four spins  $\sigma_1, \sigma_2, \sigma_3$  and  $\sigma_4$  at the corners of the plaquette but to the products  $i = \sigma_1\sigma_2, j = \sigma_2\sigma_3, k = \sigma_3\sigma_4$ , and  $l = \sigma_4\sigma_1$  on the four bonds of the plaquette. The constraint  $ijkl = 1$  should always be satisfied. However, after the truncation step of the HoTRG algorithm, the product  $ijkl = 1$  is not guarantee to take exactly the value 1. We consider a different model for which this potential difficulty does not arise. Moreover, non-local spin-spin interactions between the two Ising replicas were designed in such a way to induce a marginal critical behavior according to the mechanism proposed by Kalz *et al.* [10]. It is therefore a good way to test this mechanism.

In the first section, the model and the BTRG algorithm are presented. The phase diagram is discussed in the second section. The critical behavior along the second-order transition line is shown to belong to the Ashkin-Teller universality class in section III. Conclusions follow.

## II. MODEL AND ALGORITHM

### A. The model and its continuum limit

We consider two anti-ferromagnetic Ising models  $\sigma_{i,j}^A$  and  $\sigma_{i,j}^B$  coupled by a non-local spin-spin interaction. The Hamiltonian is

$$\begin{aligned} -\beta H = & -J_2 \sum_{i,j} \sigma_{i,j}^A [\sigma_{i+1,j}^A + \sigma_{i,j+1}^A] \\ & -J_2 \sum_{i,j} \sigma_{i,j}^B [\sigma_{i+1,j}^B + \sigma_{i,j+1}^B] \\ & + J_1 \sum_{i,j} \sigma_{i,j}^A [\sigma_{i+1,j}^B - \sigma_{i,j+1}^B] + A \leftrightarrow B \quad (5) \end{aligned}$$

The first two lines correspond to the Hamiltonian of two replicas of an anti-ferromagnetic Ising model on a square lattice. For simplicity, the two replicas lay on the same lattice. One of the two replicas can be shifted by half a lattice step in both  $i$  and  $j$  directions to get something closer to Eq. 2. The discussion that follows would not be changed. The third line of Eq. 5 is an interaction term that couples these two replicas. The interaction is ferromagnetic on horizontal edges and anti-ferromagnetic on vertical ones.  $A \leftrightarrow B$  means that the term should be repeated after the exchange of  $A$  and  $B$ . The model is depicted on Fig. 2. The phase diagram of this model is expected to display more symmetries than the original  $J_1 - J_2$  model defined by Eq. 2. It is indeed symmetric under a change of sign of  $J_1$  since the Hamiltonian is invariant under the transformation

$$J_1 \rightarrow -J_1, \quad \sigma_{i,j}^B \rightarrow -\sigma_{i,j}^B. \quad (6)$$

which amounts to a simple rotation by  $90^\circ$  of the lattice. It is also symmetric under the exchange of  $J_1$  and  $J_2$ . The Hamiltonian is indeed invariant under  $J_1 \leftrightarrow J_2$  if the spins of the two replicas are first exchanged on every two sites

$$(\sigma_{i,j}^A, \sigma_{i,j}^B) \rightarrow \begin{cases} (\sigma_{i,j}^A, \sigma_{i,j}^B), & i+j \text{ even,} \\ (\sigma_{i,j}^B, \sigma_{i,j}^A), & i+j \text{ odd} \end{cases} \quad (7)$$

and then flipped on every two lines

$$\sigma_{i,j}^{A,B} \rightarrow (-1)^i \sigma_{i,j}^{A,B}. \quad (8)$$

In the following, we will show that the Hamiltonian Eq. 5 leads to the same continuum limit as Eq. 1. The first step is to rewrite the inter-layer Hamiltonian (third and fourth lines of Eq. 5) as a sum over the plaquettes of a checkerboard lattice :

$$J_1 \sum_{\substack{i,j, \\ i+j \text{ even}}} (\sigma_{i,j}^A - \sigma_{i+1,j+1}^A) (\sigma_{i+1,j}^B - \sigma_{i,j+1}^B) + A \leftrightarrow B \quad (9)$$

Introducing the staggered magnetization  $S_{i,j}^A = (-1)^{i+j} \sigma_{i,j}^A$ , as done by Kaltz *et al.*, only changes  $J_1$  into

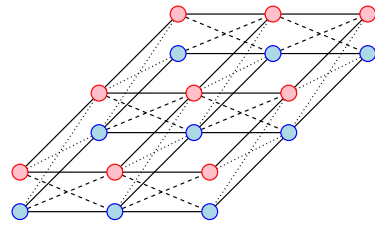


FIG. 2. Representation of the model defined by Eq. 5. For clarity, the two Ising replicas have been shifted in a third direction and represented as two layers. Red and blue circles correspond respectively to the spins  $\sigma_{i,j}^A$  and  $\sigma_{i,j}^B$ . The anti-ferromagnetic intra-layer couplings  $-J_2$  are represented as bold lines. The dashed lines are the ferromagnetic inter-layer couplings  $J_1$  and the dotted ones the anti-ferromagnetic inter-layer couplings  $-J_1$ .

$-J_1$ . As discussed above, this does not affect the phase diagram of the model. Performing now a  $45^\circ$  rotation of the lattice around the center of the plaquette, the interaction Hamiltonian becomes

$$\begin{aligned} & -J_1 \sum_{i,j} (S_{x-1/2,y}^A - S_{x+1/2,y}^A) (S_{x,y+1/2}^B - S_{x,j-1/2}^B) \\ & \simeq J_1 \int \partial_x S^A \partial_y S^B dx dy. \quad (10) \end{aligned}$$

After an integration by part, a term similar to Eq. 4 is obtained.

### B. The BTRG algorithm

The BTRG algorithm derives from the Tensor Renormalization Group (TRG) algorithm introduced by Levin and Nave [24, 25]. The original TRG algorithm was proposed first for the triangular lattice before being extended to the square lattice [26]. The starting point is a decomposition of the partition function as a product of rank 4 tensors:

$$\mathcal{Z} = \sum_{s_1, s_2, \dots} \prod_{\substack{\alpha \in V, \\ i,j,k,l \in E_\alpha}} T_{s_i s_j s_k s_l}. \quad (11)$$

A tensor  $T$  is located at each vertex  $\alpha$  of the lattice.  $E_\alpha$  denotes the subset of edges of the lattice connecting the vertex  $\alpha$  to its neighbors. Bond variables  $s_i$  are carried by the edges of the lattice. The bond variable  $s_i$  appears among the indices of the two tensors located at the vertices that are connected by the bond  $i$ . In the simple case of the Ising model, a possible decomposition of the partition function consists in identifying the bond variables  $s_i$  with the Ising spins  $\sigma_i$  (or with  $(\sigma_i + 3)/2 \in \{1, 2\}$  in the numerical implementation). The tensors  $T$  are then located at the center of the plaquettes of the square lattice and correspond to the Boltzmann weight of this plaquette:

$$T_{\sigma_i \sigma_j \sigma_k \sigma_l} = e^{\beta J (\sigma_i \sigma_j + \sigma_j \sigma_k + \sigma_k \sigma_l + \sigma_l \sigma_i)}. \quad (12)$$

This formulation makes it easy to construct the effective statistical weight  $T^{\text{eff}}$  resulting from the decimation of a spin  $\sigma_i$ .  $T^{\text{eff}}$  is given by the contraction of the two tensors at the two edges of the bond carrying the spin  $\sigma_i$

$$T_{\sigma_j \sigma_k \sigma_l \sigma'_j \sigma'_k \sigma'_l}^{\text{eff}} = \sum_{\sigma_i = \pm 1} T_{\sigma_i \sigma_j \sigma_k \sigma_l} T_{\sigma_i \sigma'_j \sigma'_k \sigma'_l}. \quad (13)$$

It is a rank 6 tensor. Iterating this procedure leads to a partition function with fewer and fewer spins but with tensors of larger and larger ranks that rapidly become unmanageable by a computer. The solution proposed by Levin and Nave relies on a Singular Value Decomposition (SVD) of each tensor before any decimation. The SVD is performed in two different ways:

$$T_{s_i s_j s_k s_l} = \begin{cases} \sum_{s_n} U_{s_i s_j s_n} \Lambda_{s_n} V_{s_k s_l s_n}, & \text{even sites,} \\ \sum_{s_n} U_{s_l s_i s_n} \Lambda_{s_n} V_{s_j s_k s_n} & \text{odd sites,} \end{cases} \quad (14)$$

for odd and even lattice sites (Fig. 3).  $U$  and  $V$  are unitary matrices that are reshaped into rank 3 tensors. Each rank 4 tensor  $T$  is replaced by the contraction of either the two rank 3 tensors  $U_{s_i s_j s_n} \sqrt{\Lambda_{s_n}}$  and  $\sqrt{\Lambda_{s_n}} V_{s_k s_l s_n}$  on even sites or  $U_{s_l s_i s_n} \sqrt{\Lambda_{s_n}}$  and  $\sqrt{\Lambda_{s_n}} V_{s_j s_k s_n}$  on odd sites. As can be seen on Fig. 3, the new tensors form a lattice with two kinds of plaquettes with either 4 or 8 sites. The 4 tensors of the plaquettes with 4 sites can be contracted, leaving a single rank 4 tensor. Performing this operation in all such plaquettes leads to a new lattice of rank 4 tensors with a lattice step larger by a factor  $\sqrt{2}$  and oriented at  $45^\circ$  of the initial one. The above-detailed procedure is exact. However, if the dimension of the tensors is initially  $\chi^4$ , the dimension of the rank 3 tensors after the SVD of Eq. 14 is  $\chi \times \chi \times \chi^2$ . After contraction, the final tensors have a dimension  $(\chi^2)^4$ . Again, after a few iterations of this algorithm, the tensors become exponentially large. To circumvent this problem, the SVD Eq. 14 can be limited to the  $\chi$  largest singular values. This truncation ensures that the dimension of the rank 3 tensors  $U$  and  $V$  are  $\chi^3$ , leading to a tensor  $T$  of dimension  $\chi^4$  after contraction. This algorithm belongs to the class of variational methods. Indeed, the truncation minimizes the error defined as the Hilbert-Schmidt norm  $\|T - T_{\text{trunc}}\|$  where  $T_{\text{trunc}}$  is the result of the truncation of  $T$ .

The accuracy of the TRG algorithm can be improved by introducing a weight  $w$  on each bond of the lattice [27]. The decomposition Eq. 11 of the partition function is replaced by

$$\mathcal{Z} = \sum_{s_1, s_2, \dots} \prod_{\substack{\alpha \in V_i \\ i, j, k, l \in E_\alpha}} T_{s_i s_j s_k s_l} \prod_i \omega_i. \quad (15)$$

The Bond-Weighted Tensor Renormalization Group algorithm (BTRG) is very similar to the TRG algorithm.

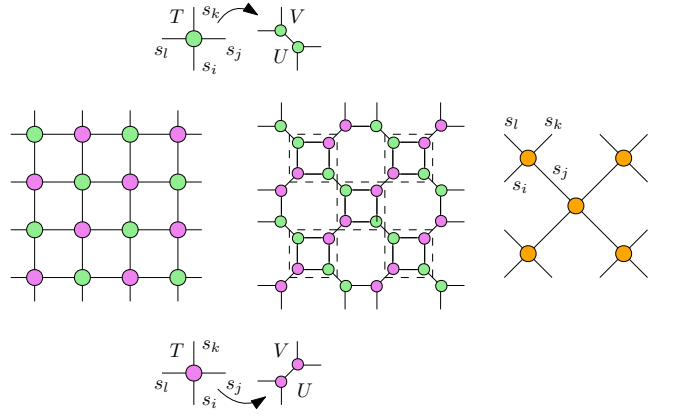


FIG. 3. TRG algorithm on the square lattice. Tensors are represented as disks with different colors on even and odd sites. The bonds between them carry the variables  $s_i$  that have to be integrated out to compute the partition function. Each variable  $s_i$  appears among the indices of the two tensors at both edges of the bond  $i$ . Above and below, the Singular Value Decomposition of the tensor  $T$  on odd and even sites allows to write the tensor  $T$  as the contraction of two rank 3 tensors  $U\sqrt{\Lambda}$  and  $\sqrt{\Lambda}V$ . In the center, the new lattice obtained after the decomposition of all tensors  $T$ . On the right, the bonds of the square plaquettes have been integrated out, leaving a square lattice of new effective tensors represented in orange color.

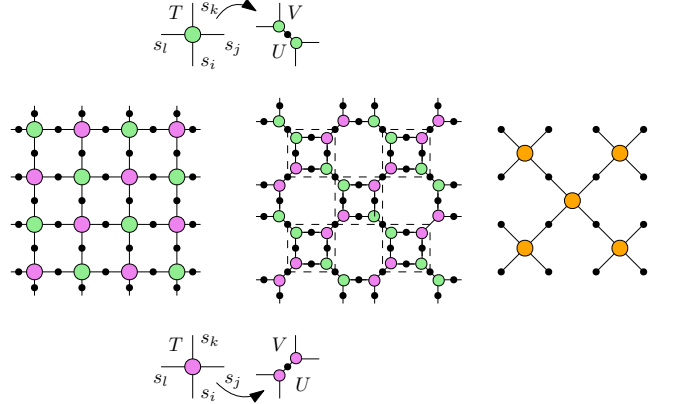


FIG. 4. BTRG algorithm on the square lattice. The difference with the TRG algorithm lies in the presence of diagonal tensors on each edge of the lattice. They are represented as black dots on the figure.

The main difference lies in the way the rank 4 tensors  $T$  are decomposed after the SVD of Eq. 14. Each tensor  $T$  is replaced by the contraction of either the two rank 3 tensors  $U_{s_i s_j s_n} (\Lambda_{s_n})^k$  and  $(\Lambda_{s_n})^k V_{s_k s_l s_n}$  on even sites or  $U_{s_l s_i s_n} (\Lambda_{s_n})^k$  and  $(\Lambda_{s_n})^k V_{s_j s_k s_n}$  on odd sites. Between these two rank 3 tensors, a new weight  $(\Lambda_{s_n})^{1-2k}$  is introduced.  $k$  is a free parameter. The TRG algorithm is recovered when  $k = 1/2$ . It was suggested that the optimal choice is  $k = -1/2$  [27]. The algorithm is depicted on Fig. 4.

Free energy and critical exponents can be estimated from the  $\chi \times \chi$  transfer matrix  $M$  of the system obtained by contraction of the tensor  $T$  [28–31]:

$$M_{s_i, s_k} = \sum_{s_j} T_{s_i s_j s_k s_j}. \quad (16)$$

The largest eigenvalues  $\lambda_i$  of the transfer matrix  $M$  are then estimated using the Lanczos algorithm as implemented in the `Arpack` library [32]. The free energy density of the system is given by the logarithm of the largest eigenvalue  $\lambda_0$ :

$$f(L) = -\frac{1}{L} \ln \lambda_0 \quad (17)$$

where the width  $L$  of the system is related to the number  $n$  of BTRG iterations by  $\sqrt{2}^n$ .

### III. PHASE DIAGRAM

#### A. Phases and transitions

The state of the system is readily determined at several points of the phase diagram. At the point  $J_1 = J_2 = 0$ , equivalent to an infinite temperature, the Ising spins are uncoupled so the equilibrium state of the system is the paramagnetic state. One may therefore assume that there exists a finite region of the phase diagram, containing the point  $J_1 = J_2 = 0$ , where the paramagnetic phase is stable. In the limit  $J_2 \rightarrow +\infty$  and  $J_1 \rightarrow 0$ , the two replicas are uncoupled and ordered anti-ferromagnetically. An anti-ferromagnetic phase is therefore expected in a region the phase diagram containing this point. The two average staggered magnetizations

$$\langle M^{A,B} \rangle = \sum_{i,j} (-1)^{i+j} \langle \sigma_{i,j}^{A,B} \rangle \quad (18)$$

are expected to take a non-zero value in this phase when a small magnetic field  $h$  is coupled to the system by a Zeeman Hamiltonian  $hM^{A,B}$ . We measured these staggered magnetizations along different lines perpendicular to the diagonal  $J_1 = J_2$  and parameterized as

$$J_1(x) = J_0 + x, \quad J_2(x) = J_0 - x \quad (19)$$

where the parameter  $x$  allows to move along these lines and  $J_0$  identifies the different lines by their intersection  $J_1 = J_2 = J_0$  with the diagonal. BTRG simulations were performed with  $\chi = 32$  states and 32 iterations for several values of the staggered magnetic field  $h$ . The staggered magnetization density is estimated from the finite-difference of the free energy density

$$\langle m^A \rangle = -\left(\frac{\partial f}{\partial h}\right)_{h \rightarrow 0^+} \simeq -\frac{f(h) - f(0)}{h}. \quad (20)$$

A stable estimate is obtained for small magnetic fields  $h \simeq 10^{-3}$ . A phase transition is clearly observed on

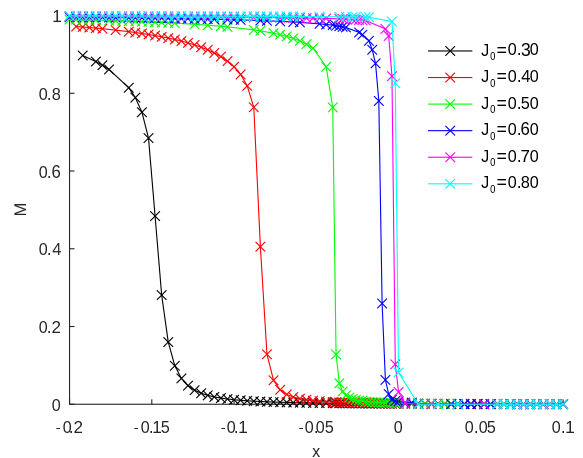


FIG. 5. Average staggered magnetization density  $\langle m^A \rangle$  along lines perpendicular to the diagonal  $J_1 = J_2$ . The staggered magnetization has been estimated by coupling a small magnetic field  $h = 10^{-3}$  to the system.

Fig. 5. The transition becomes steeper as  $J_0$  is increased. This suggests the possibility of a first-order phase at large  $J_0$ .

In the limit  $J_1 \rightarrow +\infty$  and  $J_2 \rightarrow 0$ , the Ising spins are only coupled to their neighbors in the other replica. The coupling is ferromagnetic in the horizontal direction of the lattice but anti-ferromagnetic in the vertical one. The quantity

$$\bar{M}^A = \sum_{\substack{i,j \\ \text{even}}} [\sigma_{i,j}^A + \sigma_{i+1,j}^B - \sigma_{i+1,j+1}^A - \sigma_{i,j+1}^B] \quad (21)$$

is non-zero on average when the up-down symmetry is broken by a magnetic field coupled to  $\bar{M}^A$ . Unfortunately, it is not possible to add this Zeeman coupling to our implementation of the BTRG algorithm because we assumed that all vertices of the tensor network were equivalent, while such a Zeeman coupling implies inequivalent plaquettes. Nevertheless, the behavior of  $\langle M^A \rangle$  can be deduced from the symmetry of the Hamiltonian under the exchange  $J_1 \leftrightarrow J_2$  when the transformations Eq. 7 and 8 are successively performed. One can check that the image of the order parameter Eq. 21 under these transformations is, as expected, the staggered magnetization Eq. 18. As consequence, the behavior of  $\langle \bar{M}^A(x) \rangle$  along the lines perpendicular to the diagonal  $J_1 = J_2$  is simply given by the reflection  $\langle M^A(-x) \rangle$  of the staggered magnetization.

#### B. Critical lines

As discussed above, the behavior of the staggered magnetization shows the existence of a transition line in the half plane  $J_2 > J_1$  of the phase diagram with possibly a first-order regime. Because of the symmetry

of the model under the exchange  $J_1 \leftrightarrow J_2$ , the same transition line is expected in the half-plane  $J_1 > J_2$ . In this section, we determine more precisely the location of these two transition lines in the second-order regime and study the critical behavior.

Assuming that conformal invariance holds for this system, the free energy density is expected to scale with the stripe width  $L$  as [33]

$$f(L) = f_\infty - \frac{\pi c}{6L^2} + \mathcal{O}\left(\frac{1}{L^4}\right) \quad (22)$$

at the critical point. The universal constant  $c$  is the central charge which takes the value  $c = 1/2$  for the 2D Ising model and  $c = 1$  for the Ashkin-Teller model. Away from criticality, the constant  $c$  is not universal anymore and takes a smaller value. However, it was shown to that this constant increases monotonically along the Renormalization-Group flow and is maximum at the fixed point [34]. The critical point can therefore be determined as the location of the maximum of  $c$ . We estimated the free energy density from the largest eigenvalue of the transfer matrix (Eq. 17). The central charge  $c$  is then estimated from the Finite-Size Scaling Eq. 22. To take into account the first correction to this behavior, a quadratic fit with  $1/L^2$  was performed:

$$f(L) = f_\infty - \frac{\pi c}{6L^2} + \frac{a}{L^4}. \quad (23)$$

A cubic fit does not yield significantly different results. Two difficulties were however encountered: the lattice size is multiplied by a factor  $\sqrt{2}$  at each iteration of the BTRG algorithm. As a consequence, our lattice sizes are distributed exponentially, and not linearly, as would be the case with a more traditional transfer matrix calculation. We have checked for the Ising model and the Ashkin-Teller model along its critical line that the fit gives nevertheless the expected central charge. We assume that it is also the case for our  $J_1 - J_2$  model. The second difficulty is that the free energy does not behave as  $1/L^2$  at large lattice sizes (our largest lattice size is  $\sqrt{2}^{33} \simeq 92,680$ ) but tends towards a plateau, due to the finite number of states  $\chi$  kept in the BTRG calculation and to the finite accuracy in the estimation of the largest eigenvalue  $\lambda_0$  with the `Arpack` library. To circumvent this problem, we discarded all free energies  $f(L_n)$  such that  $|f(L_n) - f(L_{n-1})| < 10^{-12}$  where  $\{L_n\}$  are the set of lattices sizes given by the BTRG algorithm. Examples of fits of the free energy density are shown on Fig. 6 for three different points on the critical line. Because the lattice sizes are distributed exponentially, logarithms are plotted. One clearly sees on Fig. 6 the plateau reached by the free energy at large lattice sizes.

The critical lines of the phase diagram have been determined by searching for the maximum of the central charge  $c$ . A rough estimate of the location of the critical lines was obtained by performing a scan of the plane

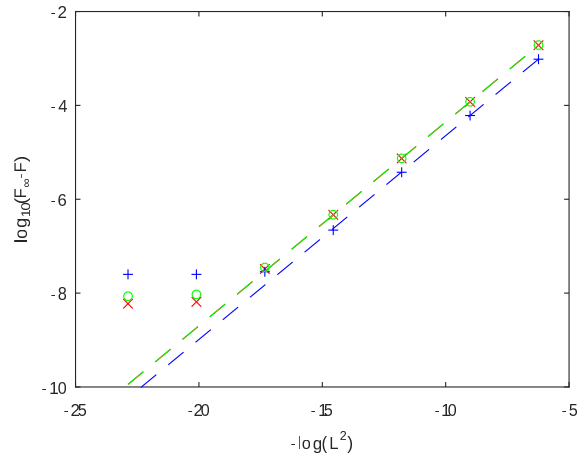


FIG. 6. Logarithm (base 10) of the free energy difference  $F_\infty - F(L)$  versus the logarithm of  $1/L^2$  for couplings  $(J_1, J_2)$  equal to  $(0.612965, -0.605170)$ ,  $(0.448669, -0.134480)$ , and  $(0.440618, 0)$ . The symbols correspond to the data points and the dashed curves to the quadratic fit. The central charge  $c$  is related to the vertical intercept. The number of states is  $\chi = 48$ .

$(J_1, J_2)$  while keeping only  $\chi = 16$  states in the BTRG algorithm. The location of the maxima was then refined by dichotomy until reaching an accuracy of  $10^{-5}$ . A few points around the maxima were selected and used to initiate a new search by dichotomy with  $\chi = 24$  states. The procedure was repeated for 32 and 48 states. The central charge is plotted for  $\chi = 16$  in Fig. 7. Two branches are clearly observed. As expected (Sec. II A), they are images of each other under the exchange  $J_1 \leftrightarrow J_2$ . The two branches seem to merge at  $J_1 = J_2 \simeq 0.6$ . Beyond this point, i.e. for  $J_1 \gtrsim 0.6$ , the free energy density  $f(L)$  reaches a plateau already for small lattice sizes  $L$  so that no fit can be performed. For  $\chi = 24$ , the free energy density  $f(L)$  can be fitted only for  $J_1 \lesssim 0.40$  (first branch) or  $J_2 \lesssim 0.40$  (second branch). For  $\chi = 32$  and 48, the fit is reliable only for  $J_1 \lesssim 0.33$  (first branch) or  $J_2 \lesssim 0.33$  (second branch). In contrast to the case  $\chi = 16$ , the two branches do not merge anymore. This does not imply that there is no phase transition for  $J_1 \gtrsim 0.33$ . A phase transition was indeed observed in Sec. III A. However, the relation Eq. 17 holds only for second-order phase transitions when the RG fixed point is conformally invariant. The phase transition beyond  $J_1 \gtrsim 0.33$  is therefore probably of first order.

The maxima of the central charge are plotted in the two branches on Fig. 8. For  $\chi = 16$ , the central charge is approximately constant for  $J_1, J_2 \lesssim 0.4$ , then decreases rapidly and vanishes for  $J_1, J_2 \simeq 0.6$ . For  $\chi = 24, 32$  and 48, this decrease is much less pronounced. Instead, the central charge varies slowly from  $c = 0.9774$  at  $(J_1, J_2)$  equal to  $(0, -0.44062)$  and  $(0.44062, 0)$  [36] to  $c = 0.9383$  at  $(J_1, J_2)$  equal to  $(0.33620, -0.49206)$  and  $(0.49206, -0.33620)$  for  $\chi = 48$ . Close values are ob-

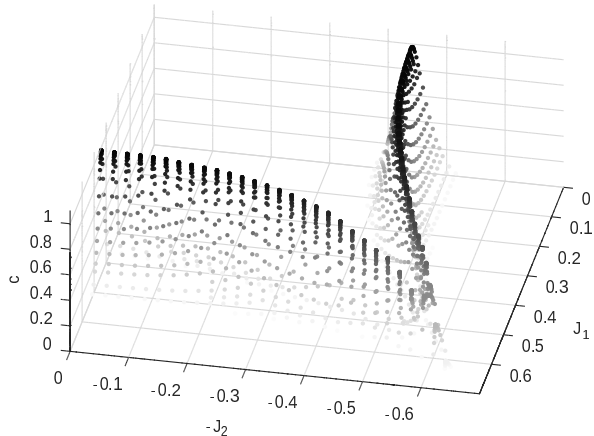


FIG. 7. Central charge  $c$  versus the couplings  $J_1$  and  $-J_2$  for  $\chi = 16$  states in the BTRG algorithm.

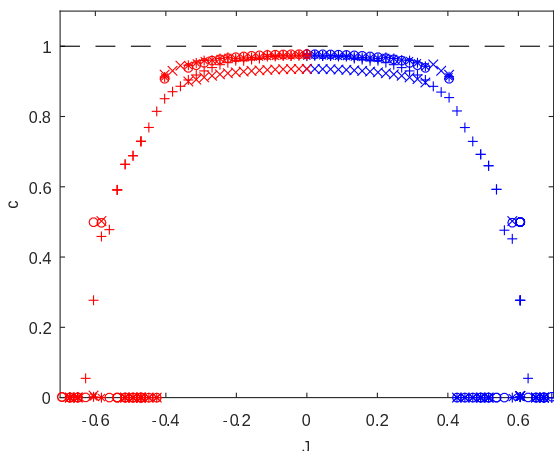


FIG. 8. Maximum of the central charge  $c$  in the two branches versus the coupling  $J_1$  in the first branch (blue symbols) and versus  $-J_2$  in the second branch (red symbols). The different symbols correspond to different number of states ( $\chi = 16$  for  $+$ , 24 for  $\times$ , 32 for  $*$  and 48 for  $\circ$ ).

tained for  $\chi = 32$  while much larger deviations are observed for  $\chi = 24$ . Surprisingly, a few points at  $c \simeq 0.498$  around  $(J_1, J_2) \simeq (0.61, -0.59)$  and  $(0.59, -0.61)$  can be seen on the figure for  $\chi = 48$  but not for the other number of states. The free energy density of one of these points is plotted on Fig. 6. Nothing special can be observed. Our interpretation is that, probably due to a numerical instability, the BTRG algorithm took the system to a fixed point which is critical for one of the two replicas but trivial (either paramagnetic or anti-ferromagnetic) for the other.

In the Ashkin-Teller model, the central charge is expected to remain constant at  $c = 1$  along the self-dual critical line. Our numerical data for the  $J_1 - J_2$  Ising model show deviations that are at most 6% from this

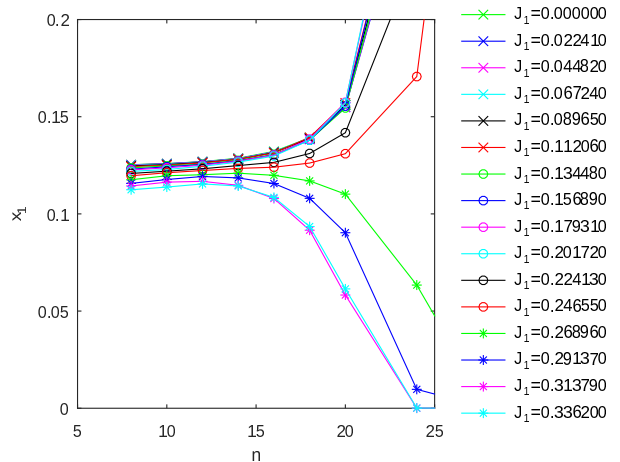


FIG. 9. First scaling dimension  $x_1$  versus the number of iterations of the BTRG algorithm with  $\chi = 96$ . The different curves correspond to different points on the first critical line.

value.

#### IV. CRITICAL BEHAVIOR

The scaling dimensions  $x_n$  of the scaling operators of the theory can be estimated from the gaps between the eigenvalues  $\lambda_n$  of the transfer matrix and the largest one  $\lambda_0$ . The gap-exponent relation states that

$$x_n = -\frac{L}{2\pi} \ln \frac{\lambda_n}{\lambda_0}. \quad (24)$$

To improve the accuracy on the  $x_n$ , additional calculations were performed with  $\chi = 64$  and 96 states along the two critical lines previously determined with  $\chi = 48$ . As discussed in details in Ref. [29], the estimation of the scaling dimensions require to choose carefully the lattice size. At too small lattice sizes, Finite-Size corrections cannot be neglected and yield systematic deviations of the estimated scaling dimensions. At intermediate lattice sizes, a plateau is observed on Fig 9 for various points on the critical line. However, at large lattice sizes, the estimates of the scaling dimensions either diverge or tends to zero, as would be case in the ferromagnetic or paramagnetic case. Due to the finite number of states  $\chi$  kept in the BTRG algorithm, the system is indeed gapped and not really critical. We measured the scaling dimensions in the plateau, after 12 iterations of the BTRG algorithm.

The three first scaling dimensions along the two critical curves are plotted on Fig. 10. The difference between the first two scaling dimensions  $x_1$  and  $x_2$  is at most  $4.10^{-4}$  so it can be assumed that they are degenerated. They take a value close to  $1/8$  at the points  $(0, \frac{1}{2} \ln(1 + \sqrt{2}))$  and  $(-\frac{1}{2} \ln(1 + \sqrt{2}), 0)$  where the two Ising replicas are not coupled. When going away from these points, they decrease down to a value 0.118 at

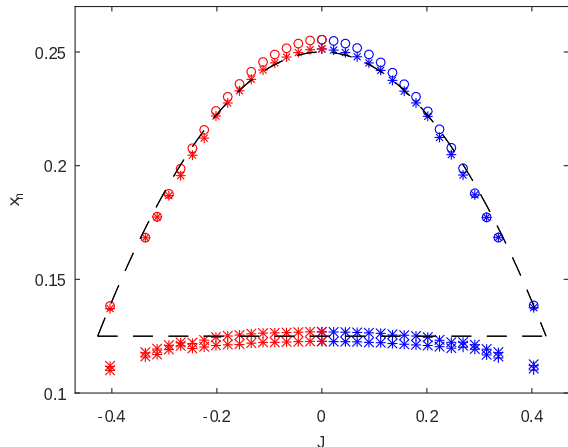


FIG. 10. Three first scaling dimensions  $x_n$  along the two critical lines versus the coupling  $J_1$  in the first branch (blue symbols) and versus  $-J_2$  in the second branch (red symbols). The different symbols correspond to  $n = 1$  for  $\circ$ , 2 for  $\times$  and 3 for  $\ast$ . The black dashed curves are only guide to the eyes.

$\chi = 64$  and 0.116 at  $\chi = 96$ , i.e. a relative deviation of 6% from  $1/8$ . Note that the same decrease was observed for the central charge. Assuming that  $x_1$  and  $x_2$  are constant and equal to  $x_\sigma = 1/8$ , one can associate them to the magnetization density of each Ising replicas.

As can be observed on Fig. 10, the third scaling dimension  $x_3$  takes the value 0.254 at  $\chi = 64$  and 0.255 at  $\chi = 96$ , close to  $1/4$ , at the points where the Ising replicas decouple and decreases significantly along the two critical lines. Remarkably, the data points fall reasonably close to a simple parabola  $\frac{1}{4} - \frac{1}{8}(J_1/J_t)^2$  with  $J_t \simeq 0.427$ . The range of variation of the third scaling dimension  $x_3$  is similar to that of the scaling dimension  $x_{\sigma\tau}$  of the polarization density of the Ashkin-Teller model, which decreases along the self-dual critical line, going from  $1/4$  at the Ising point to  $1/8$  at the 4-state Potts point. If the similarity is actually a correspondence, it would imply that our  $J_1 - J_2$  model belongs to the 4-state Potts universality class when  $J_1 = J_t$  (resp.  $J_2 = J_t$ ) on the first (resp. second) branch.

The fact that the third scaling dimension goes from  $1/4$  to  $1/8$ , like the scaling dimension  $x_{\sigma\tau}$  of the polarization density of the Ashkin-Teller model, is not sufficient to declare that our  $J_1 - J_2$  model belongs to the Ashkin-Teller universality class. In the latter, the critical exponents have been shown to be [14–16]

$$x_\sigma = \frac{1}{8}, \quad x_{\sigma\tau} = \frac{1}{8-4y}, \quad y_t = \frac{3-2y}{2-y} \quad (25)$$

where the parameter  $y$  is in the range  $[0; 3/2]$  along the critical line. Using the ansatz  $x_{\sigma\tau} = \frac{1}{4} - \frac{1}{8}(J_1/J_t)^2$  that was introduced above, we extracted the parameter  $y$  and plotted the scaling dimension  $x_t = 2 - y_t$  of the energy density. As can be observed on Fig. 11, the de-

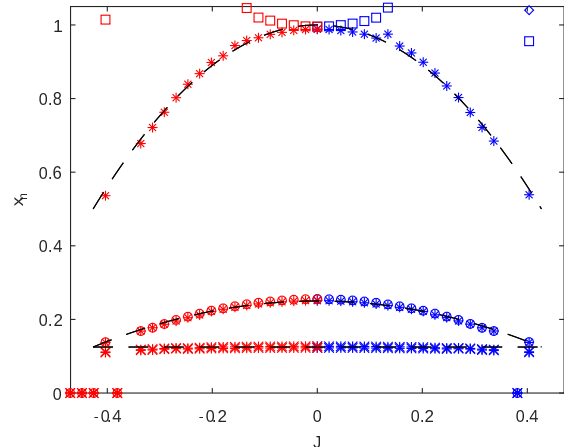


FIG. 11. Five first scaling dimensions  $x_n$  along the two critical lines versus the coupling  $J_1$  in the first branch (blue symbols) and versus  $-J_2$  in the second branch (red symbols). The black dashed curves are only guide to the eyes. The dashed curve for  $x_4$  ( $\ast$ ) has been computed using a parabolic approximation of  $x_3$  ( $\circ$ ) and the assumption of a Ashkin-Teller universality class.

pendence on  $J_1$  (resp.  $J_2$ ) of the 4th scaling dimensions of our  $J_1 - J_2$  model is in good agreement with this prediction of  $x_t$ . This provides strong evidence that the model belongs to the Ashkin-Teller universality class.

One can see on the figure that the gap with the 5th scaling dimension vanishes at the Ising point for  $\chi = 96$ . It is a pure coincidence. For  $\chi = 64$ , the 5th scaling dimension  $x_5$  takes a value close to  $\simeq 0.92$ . A crossing with the 4th scaling dimensions is therefore observed for  $J_1 \simeq 0.13$ . For  $\chi = 48$ ,  $x_5 \simeq 0.82$  and the crossing with  $x_4$  occurs at larger couplings  $J_1$ . We therefore expect that, for  $\chi > 96$ , the 5th scaling dimension take values larger than 1 so that the gap with  $x_4$  does not close anymore. One should also mention that, as discussed earlier, the estimation of the critical line is reliable only for  $J_1 \lesssim 0.33$  or  $J_2 \lesssim 0.33$ . As a consequence, all scaling dimensions  $x_n$  computed for  $J_1 > 0.33$  or  $J_2 > 0.33$  take values either very small or very large and, in this case, are not visible on the figure. Surprisingly, the two points at  $J_1 \simeq 0.40344$  and  $J_2 \simeq 0.40344$  are an exception and lead to estimates of the scaling dimensions  $x_n$  consistent with the Ashkin-Teller universality class.

## V. CONCLUSIONS

In this study, we have explored the phase diagram of a new 2D frustrated Ising model with non-local spin-spin interactions sharing the same continuum limit as the  $J_1 - J_2$  model. Using the BTRG Tensor-Network algorithm, we have provided evidence that the two transition lines, related by the symmetry  $J_1 \leftrightarrow J_2$ ,



include both a first and a second-order regime. Even though our model is identical to the  $J_1 - J_2$  model only in the scaling limit, implying that only universal quantities are expected to match in the two models, our conclusions tend to be in line with most studies on the  $J_1 - J_2$  model and contradict the iTeBD study that concluded to a second-order regime limited to the point  $J_1 = 0$  of the phase diagram [21].

In the second-order regime, our estimates of the central charge and of the magnetic, electric, and thermal critical exponents along the critical line are compatible with the Ashkin-Teller universality class. This result is in agreement with the Monte Carlo simulations performed one decade ago [10–13] but not with the more recent Tensor-

Network calculations [18, 19]. This also demonstrates the validity of the analysis of the scaling limit of the  $J_1 - J_2$  model reported in Ref. [10].

## ACKNOWLEDGMENTS

This work was supported by the french ANR-PRME UNIOOPEN grant (ANR-22-CE30-0004-01).

## VI. BIBLIOGRAPHY

- 
- [1] J. Cardy, *Scaling and Renormalization in Statistical Physics*, Cambridge University Press, Cambridge, (1996)
- [2] G. Mussardo, *Statistical Field Theory: An Introduction to Exactly Solved Models in Statistical Physics*, Oxford University Press, Oxford, (2020).
- [3] M. P. Nightingale, *Non-Universality for Ising-like Spin Systems*, Physics Letters A **59**, 486 (1977).
- [4] R. H. Swendsen and S. Krinsky, *Monte Carlo Renormalization Group and Ising Models with  $n \lesssim 2$* , Phys. Rev. Lett. **43**, 177 (1979).
- [5] K. Binder and D. P. Landau, *Phase Diagrams and Critical Behavior in Ising Square Lattices with Nearest- and next-Nearest-Neighbor Interactions*, Phys. Rev. B **21**, 1941 (1980).
- [6] J. Oitmaa, *The Square-Lattice Ising Model with First and Second Neighbour Interactions*, J. Phys. A: Math. Gen. **14**, 1159 (1981).
- [7] M. Suzuki, *New Universality of Critical Exponents*, Progress of Theoretical Physics, **51**, 1992 (1974).
- [8] J. L. Morán-López, F. Aguilera-Granja, and J. M. Sanchez, *First-Order Phase Transitions in the Ising Square Lattice with First- and Second-Neighbor Interactions*, Phys. Rev. B **48**, 3519 (1993).
- [9] J. L. Morán-López, F. Aguilera-Granja, and J. M. Sanchez, *Phase Transitions in Ising Square Antiferromagnets with First- and Second-Neighbour Interactions*, J. Phys.: Condens. Matter **6**, 9759 (1994).
- [10] A. Kalz, A. Honecker, and M. Moliner, *Analysis of the Phase Transition for the Ising Model on the Frustrated Square Lattice*, Phys. Rev. B **84**, 174407 (2011).
- [11] S. Jin, A. Sen, and A. W. Sandvik, *Ashkin-Teller Criticality and Pseudo-First-Order Behavior in a Frustrated Ising Model on the Square Lattice*, Phys. Rev. Lett. **108**, 045702 (2012).
- [12] A. Kalz and A. Honecker, *Location of the Potts-Critical End Point in the Frustrated Ising Model on the Square Lattice*, Phys. Rev. B **86**, 134410 (2012).
- [13] S. Jin, A. Sen, W. Guo, and A. W. Sandvik, *Phase Transitions in the Frustrated Ising Model on the Square Lattice*, Phys. Rev. B **87**, 144406 (2013).
- [14] L. P. Kadanoff, *Connections between the Critical Behavior of the Planar Model and That of the Eight-Vertex Model*, Phys. Rev. Lett. **39**, 903 (1977).
- [15] B. Nienhuis, *Critical Behavior of Two-Dimensional Spin Models and Charge Asymmetry in the Coulomb Gas*, J Stat Phys **34**, 731 (1984).
- [16] R. J. Baxter, *Exactly solved models of statistical mechanics*, Academic Press, Londres (1982)
- [17] Z. Y. Xie, J. Chen, M. P. Qin, J. W. Zhu, L. P. Yang, and T. Xiang, *Coarse-graining renormalization by higher-order singular value decomposition*, Phys. Rev. B **86**, 045139 (2012).
- [18] H. Li and L.-P. Yang, *Tensor network simulation for the frustrated  $J_1 - J_2$  Ising model on the square lattice*, Phys. Rev. E **104**, 024118 (2021)
- [19] K. Yoshiyama and K. Hukushima, *Higher-Order Tensor Renormalization Group Study of the  $J_1 - J_2$  Ising Model on a Square Lattice*, Phys. Rev. E **108**, 054124 (2023).
- [20] S.-W. Li and F.-J. Jiang, *A Comprehensive Study of the Phase Transitions of the Frustrated  $J_1 - J_2$  Ising Model on the Square Lattice*, Progress of Theoretical and Experimental Physics 053A06 (2024).
- [21] A. A. Gangat, *Weak First-Order Phase Transitions in the Frustrated Square Lattice  $J_1 - J_2$  Classical Ising Model*, Phys. Rev. B **109**, 104419 (2024).
- [22] W. Janke, *Monte Carlo Simulations in Statistical Physics — From Basic Principles to Advanced Applications*, in Order, Disorder and Criticality, World Scientific (2012)
- [23] C. Chatelain, *CTMRG study of the critical behavior of an interacting-dimer model*, J. Stat. Mech. **2024**, 083201 (2024).
- [24] M. Levin and C. P. Nave, *Tensor Renormalization Group Approach to 2D Classical Lattice Models*, Physical Review Letters **99**, 120601 (2007).
- [25] T. Xiang, *From Density Matrix and Tensor Network Renormalization*, Cambridge University Press, Cambridge, (2023)
- [26] Z.-C. Gu and X.-G. Wen, *Tensor-Entanglement-Filtering Renormalization Approach and Symmetry Protected Topological Order*, Phys. Rev. B **80**, 155131 (2009).
- [27] D. Adachi, T. Okubo, and S. Todo, *Bond-Weighted Tensor Renormalization Group*, Phys. Rev. B **105**, L060402 (2022).
- [28] A. Ueda and M. Oshikawa, *Finite-Size and Finite Bond Dimension Effects of Tensor Network Renormalization*, Phys. Rev. B **108**, 024413 (2023).

- [29] A. Ueda, *Renormalization Group Flow and Fixed-Point in Tensor Network Representations*, Ph.D dissertation, univ. Tokyo, [arXiv:2401.18068](https://arxiv.org/abs/2401.18068).
- [30] C.-Y. Huang, S.-H. Chan, Y.-J. Kao et P. Chen, *Tensor network based finite-size scaling for two-dimensional Ising model*, Phys. Rev. B **107**, 205123 (2023).
- [31] W. Guo, and T.-C. Wei, *Tensor network methods for extracting conformal field theory data from fixed-point tensors and defect coarse graining*, Phys. Rev. E **109**, 034111 (2024).
- [32] R. B. Lehoucq, D. C. Sorensen, and C. Yang, *ARPACK Users' Guide*, Society for Industrial and Applied Mathematics (1998)
- [33] H. W. J. Blöte, J. L. Cardy and M. P. Nightingale, *Conformal invariance, the central charge, and universal finite-size amplitudes at criticality*, Phys. Rev. Lett. **56**, 742 (1986).
- [34] A.B. Zamolodchikov, *Irreversibility of the flux of the renormalization group in a 2D field theory*, JETP Lett. **43**, 730 (1986).
- [35] Note that the two Ising replicas decouple at the points  $(0, -\frac{1}{2} \ln(1 + \sqrt{2})) \simeq (0, -0.44069)$  and  $(\frac{1}{2} \ln(1 + \sqrt{2}), 0)$  of the transition lines.
- [36] Note1